Appl Magn Reson (2017) 48:827–840
DOI 10.1007/s00723-017-0903-z

Applied Magnetic Resonance

ORIGINAL PAPER

High-Field Electron Paramagnetic Resonance Reveals a Stable Glassy Fraction up to Melting in Semicrystalline Poly(dimethylsiloxane)

Carlo Andrea Massa[1] · Silvia Pizzanelli[2] · Vasile Bercu[3] · Luca Pardi[1] · Dino Leporini[1,4]

Received: 17 March 2017 / Revised: 18 May 2017 / Published online: 1 June 2017

Abstract The reorientation of the guest 4-methoxy-TEMPO (spin probe) in the disordered fraction of semicrystalline poly(dimethylsiloxane) (PDMS) is investigated by high-field electron paramagnetic resonance (HF-EPR) at 190 and 285 GHz. Accurate numerical simulations of the HF-EPR lineshapes evidence that the reorientation times of the spin probes are distributed between the melting temperature T_m and T_m—30 K. The distribution exhibits, in addition to a broad component, a narrow component with low mobility up to the PDMS melting point. It is shown that the temperature dependence of the reorientation time of the spin probes with low mobility is the same of the spin probes in glassy PDMS. The result suggests that the low-mobility fraction is localized in the so-called rigid amorphous fraction.

1 Introduction

In a semicrystalline polymer (SCP), the macromolecules pack together in ordered regions called crystallites which are separated by disordered non-crystalline regions [1, 2]. Recently, an intermediate interfacial region between crystallites and disordered surroundings, usually referred to as rigid amorphous fraction (RAF),

✉ Dino Leporini
dino.leporini@unipi.it

[1] Istituto per i Processi Chimico-Fisici-Consiglio Nazionale delle Ricerche (IPCF-CNR), via G. Moruzzi 1, 56124 Pisa, Italy

[2] Istituto di Chimica dei Composti Organometallici-Consiglio Nazionale delle Ricerche (ICCOM-CNR), via G. Moruzzi 1, 56124 Pisa, Italy

[3] Department of Physics, University of Bucharest, Str. Atomistilor 405, Magurele, Jud. Ilfov, 077125 Bucharest, Romania

[4] Dipartimento di Fisica "Enrico Fermi", Universitá di Pisa, Largo B. Pontecorvo 3, 56127 Pisa, Italy

has been evidenced [1, 3, 4]. The non-crystalline region other than RAF is expected to exhibit properties like the amorphous bulk polymers and is usually termed as mobile amorphous fraction (MAF). MAF becomes liquid-like above T_g, whereas RAF devitrifies even close to or above the melting temperature T_m [3, 5]. RAF has been observed long time ago also in one of the most flexible polymers known: poly(dimethylsiloxane) (PDMS) [6].

To make clear distinction between disordered regions, structural studies are little informative owing to the small differences of disordered structures [7]. In contrast, more insight is provided by techniques sensitive to mobility variations like nuclear magnetic resonance (NMR) [8, 9], dielectric relaxation [10], or measurements of the solubility of a gas; for a review, see Ref. [4]. Following the same approach, earlier [11, 12] and novel [13, 14] investigations of SCPs addressed the rotational mobility of suitable guest radicals (spin probes) in SCPs. They are carried out by electron paramagnetic resonance (EPR) [15], in particular high-field EPR (HF-EPR) [13, 14], and exploit the expertise gained on both semicrystalline materials like ice-water mixtures [16–21] and amorphous polymers [22–30]. One major advantage in using guest molecules to investigate SCPs is their selectivity. In fact, assignment of a relaxation process to the amorphous, crystalline, or interfacial regions of SCPs is a delicate matter [9, 22, 23, 31–35]. From this respect, one has to notice that the crystallites are very often impermeable even to small molecules which are expelled by the ordered regions during the crystallization [36–39]. The confinement of small tracer molecules in the disordered fraction offers the possibility of selective studies of such regions in SCPs. It is worth noting that we do not expect dramatic changes in the mobility of the spin probes in MAF and RAF. This motivated us to resort to HF-EPR, which is more challenging than the customary X-band EPR, but it offers remarkable orientation resolution as far as the statics and the dynamics of the spin probes are concerned [27, 40, 41].

In a previous HF-EPR study [13], we investigated the constrained and heterogeneous dynamics in the MAF and RAF fractions of slowly cooled PDMS. It was concluded that RAF is larger than MAF around T_g, whereas RAF is a small amount of the total amorphous phase at $T_m - 19$ K. No RAF was detected above $T_m - 19$ K and no distinctive spectral features associated with RAF were observed at any temperature. In the present study, an improved strategy to increase both the amount of RAF as well as the coupling between the spin probe and PDMS has been devised. As a consequence, we observed well-defined signatures of RAF in the HF-EPR lineshape and provide evidence of RAF persisting up to T_m.

The paper is organized as follows. In Sect. 2, experimental details are given. Section 3 discusses the results. The main conclusions are summarized in Sect. 4.

2 Experimental Section

2.1 Sample

PDMS and the paramagnetic tracers 2,2,6,6-tetramethyl-1-piperidinyloxy (TEMPO) and 4-methoxy-2,2,6,6-tetramethyl-1-piperidinyloxy (mTEMPO) were purchased

from Aldrich and used as received. The chemical structures of the spin probes are given in Fig. 1. Their size is quite similar to the one of the PDMS monomers which, in turn, is quite close to the Kuhn length owing to the high flexibility of PDMS. The weight-average molecular weight M_w of PDMS was 90,200 g/mol and polydispersity, M_w/M_n, was 1.96. The samples (about 0.5 cm^3) were prepared by dissolving TEMPO or mTEMPO and PDMS in chloroform according to the solution method [42]. Then, the solution was heated at about 330 K for 24 h and no residual chloroform was detected by NMR. In both samples, the spin probe concentration was less than 0.05% in weight. Differential scanning calorimetry (DSC) measurements, detailed elsewhere [14], provide the following transitions: glass transition (T_g) at 148 K, cold crystallization (T_{cc}) at about 184 K, and melting onset at about 209 K with $T_m \simeq 230$ K. The crystallinity fraction is expected in the range 30–60 %.

2.2 Thermal Protocol

The sample was preliminarily quenched in liquid nitrogen and put in a Teflon holder. Then, the holder was placed in a single-pass probe cell, and finally, the whole system was loaded cold into the cooled EPR cryostat. All the HF-EPR data were collected during the subsequent slow heating. The sample was kept about 1 hour at each temperature before the EPR spectrum acquisition. The present protocol is expected to yield a larger amount of RAF compared to slow cooling from the melt [13, 14]. In fact, as reported in polymers [45, 46], as well as supercooled water [19–21], quench cooling in the glass region and subsequent re-heating to reach the temperature of interest T ($T_g < T < T_m$) lead to larger polycrystallinity than slow cooling from above T_m down to T. The enhancement is understood in terms of both augmented primary nucleation and increased disorder of the larger, crystallite surfaces, thus anticipating a larger amount of RAF, considering that the RAF thickness is weakly dependent on both the temperature and the crystallinity [1].

The cooling protocol adopted here is different from the one of our previous study of PDMS where the sample was slowly cooled below the glass transition [13, 14]. Henceforth, we shortly name the PDMS obtained with the two cooling protocols as $PDMS_q$ (quench cooled) and $PDMS_{sc}$ (slowly cooled). In Table 1, the distinctive characteristics of the two samples are shortly summarized.

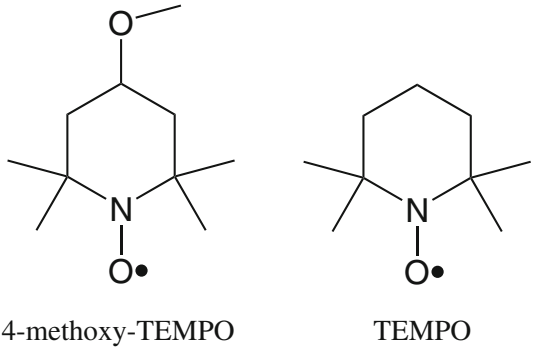

Fig. 1 Chemical structures of the guest paramagnetic probes mTEMPO ($V = 197$ Å^3) [43] and TEMPO ($V = 171$ Å^3) [43]. The size of both mTEMPO ($V^{1/3} = 0.58$ nm) and TEMPO ($V^{1/3} = 0.56$ nm) is comparable to the monomer size $v_m^{1/3} = 0.51$ nm and the Kuhn length $\ell_K = 0.50$ nm of PDMS [44]

Table 1 Distinctive characteristics of the samples examined

Sample name	Cooling protocol	Spin probe	References
$PDMS_q$	Sample prequenched in liquid nitrogen from the melt and loaded cold into the cryostat	mTEMPO	This work
$PDMS_{sc}$	Sample cooled from the melt to 124 K with a rate of 1 K/min	TEMPO	[13]

In both cases, the spectra were recorded stepwise at increasing temperatures upon slow heating

2.3 EPR Measurements

The EPR experiments were carried out on an ultrawideband EPR spectrometer which is detailed elsewhere [47]. Basically, the source is a 95 GHz Gunn effect oscillator which may be doubled or tripled in frequency at 190 and 285 GHz, respectively. To transmit millimeter-wave power metallic, oversized waveguides are used. These are overmoded waveguides which are copper cylindrical pipes with an internal diameter of 10 mm guiding the radiation to a single-pass non-resonant sample holder. A Nb_3Sn and NbTi Oxford superconductor magnet generates a magnetic field with intensity up to 12 T with field homogeneity equal to 10 ppm. With the purpose of increasing the signal-to-noise ratio, amplitude modulation of the magnetic field is performed with frequency of 10 KHz and amplitude of about 1 G. The EPR signal is detected by a InSb bolometer operating at liquid He temperature and decoded by a lock-in. A cryostat by Oxford Instruments operating in a liquid He flow controls the temperature of the probe head.

2.4 Data Analysis

The spin probe mTEMPO has one unpaired electron with spin $S = 1/2$ subject to hyperfine coupling to ^{14}N nucleus with spin $I = 1$. For the calculation of the lineshapes, we used numerical routines described elsewhere [48]. The **g** and hyperfine **A** tensor interactions were assumed to have the same principal axes. The x axis is parallel to the N–O bond, the z axis is parallel to the nitrogen and oxygen 2π orbitals, and the y axis is perpendicular to the other two. The principal components of the two tensors (g_{xx}, g_{yy}, g_{zz}, A_{xx}, A_{yy}, and A_{zz}) are input parameters to calculate the EPR lineshape. They were carefully measured by simulating the "powder" spectrum, i.e., that recorded at very low temperature, where the lineshape is not influenced by the tracer reorientation. A_{xx} and A_{yy} values are affected by a large uncertainty, because they are small compared to the linewidth. To obtain more reliable values, we used the additional constraint $\frac{1}{3}(A_{xx} + A_{yy} + A_{zz}) = A_{iso}$, with A_{iso} being the hyperfine splitting observed in the melt at 255 K and assumed that $A_{xx} = A_{yy}$. The best-fit magnetic parameters are $g_{xx} = 2.0096$, $g_{yy} = 2.0058$, $g_{zz} = 2.0017$, $A_{xx} = A_{yy} = 0.62$ mT, and $A_{zz} = 3.37$ mT. In all the simulations, the principal components of the tensors were set to these values.

To keep the number of adjustable parameters as limited as possible, the tracer reorientation is modelled as isotropic diffusion, characterized by the rotational

reorientation time τ_{SRT}, which is related to the rotational diffusion coefficient D through the equation $\tau_{SRT} = \frac{1}{6D}$. The extension of the model to account for possible anisotropic rotational diffusion of the guest molecule, as, e.g., outlined in Ref. [49], was deemed unnecessary, given the nearly spherical shape of mTEMPO, see Fig. 1, as also concluded in other studies with the conventional and high-field EPR concerning nearly identical spin probes [41].

The theoretical lineshape was convoluted with a Gaussian function with a width of 2 G to account for the inhomogeneous broadening. The spectra expected when a distribution of reorientation times occurs were calculated summing up about 600 spectra characterized by reorientation times in the range 0.01–300 ns, each spectrum being weighted according to the distribution parameters. The best-fit parameters and related uncertainties were obtained by routine procedures.

3 Results and Discussion

3.1 HF-EPR Lineshapes of mTEMPO in $PDMS_q$

Figure 2 (upper trace) compares the lineshapes of mTEMPO and TEMPO gathered at nearly the same temperature above T_m where there is no difference between $PDMS_q$ and $PDMS_{sc}$, differing only in the features of the crystalline fractions. At such high temperatures, the HF-EPR lineshapes are heavily affected (narrowed) by the fast reorientation of the spin probes. However, the larger linewidths of the mTEMPO lineshape evidence that the reorientation is slower than the one of TEMPO. The same conclusion is reached at lower temperatures. In fact, the middle and lower panels of Fig. 2 compare the lineshapes of mTEMPO and TEMPO at temperatures where the central peak exhibits the same shape. It is seen that, even if the temperature of the mTEMPO sample is higher, the lineshape of mTEMPO exhibits more pronounced powder-like features than TEMPO, suggesting lower rotational mobility.

Additional evidence about the faster dynamics of TEMPO in $PDMS_{sc}$ with respect to mTEMPO in $PDMS_q$ is provided in Fig. 3 where some spectral features are analyzed. In fact, the linewidth of the three outermost lines on the right-hand side of the lineshape of mTEMPO changes little below the glass transition and starts increasing above $T_g + 10$ K, whereas in the case of TEMPO in $PDMS_{sc}$, the increase starts below T_g due to the higher mobility, see Ref. [14]. Figure 3 also shows that the parameter ΔB, defined in the caption of Fig. 2, exhibits considerable temperature dependence, especially above T_g. According to the previous analysis [29], this finding suggests that the reorientation of mTEMPO proceeds by small angles and prompted us to adopt the diffusion model, as outlined in Sect. 2.4.

3.2 Coupling Between PDMS and the Spin Probe

In Sect. 3.1, evidence of a slower reorientation time of mTEMPO in $PDMS_q$ in comparison to TEMPO in $PDMS_{sc}$ is provided even in the absence of crystalline fraction. We remind that $PDMS_q$ and $PDMS_{sc}$ differ only in the features of the

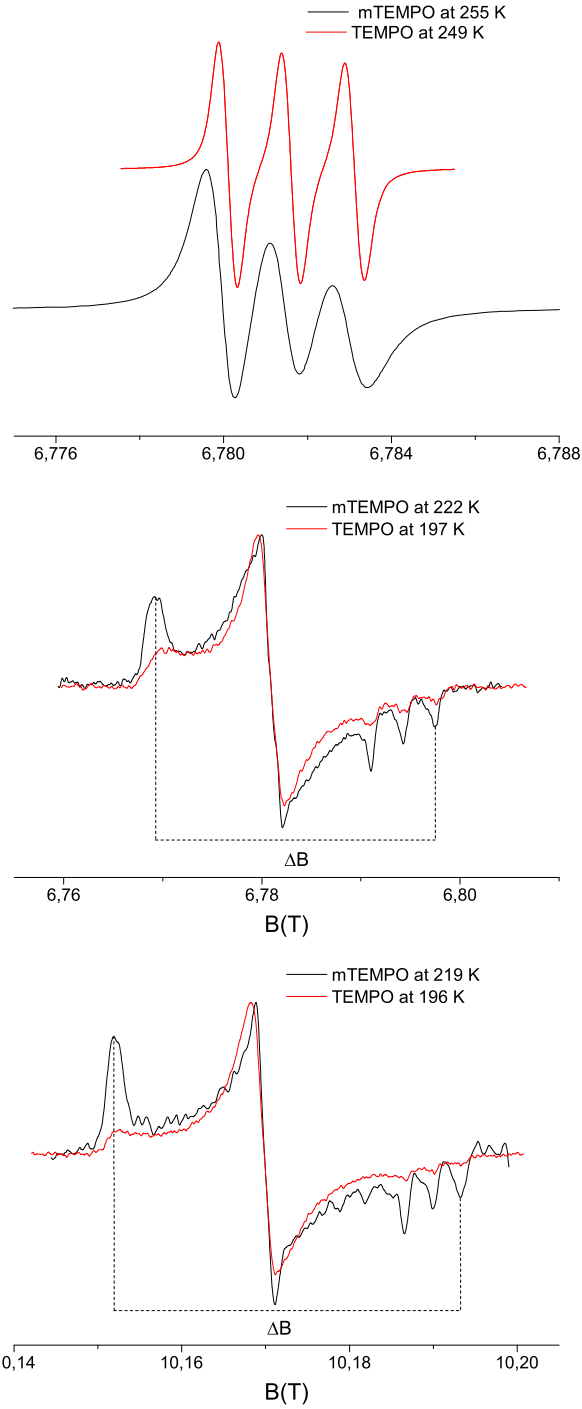

Fig. 2 *Top* HF-EPR spectra at 190 GHz of mTEMPO in $PDMS_q$ and TEMPO in $PDMS_{sc}$ recorded at $T_m + 25$ K and $T_m + 19$ K, respectively. *Middle* HF-EPR spectra at 190 GHz of the spin probes in $PDMS_q$ and $PDMS_{sc}$ at the indicated temperatures. *Bottom* as in *middle panel* with HF-EPR at 285 GHz. The temperatures of the *middle* and *bottom panels* are chosen to match the central peaks of the lineshape. ΔB, indicated in those panels, is the difference between the resonating magnetic fields of the outermost peaks observed at lower temperatures

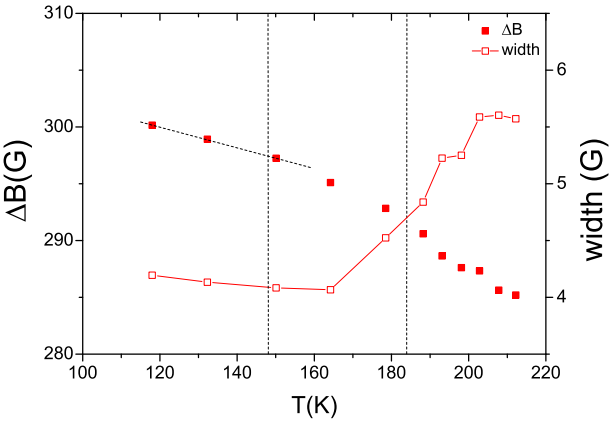

Fig. 3 Temperature dependence of ΔB (*filled squares*), defined in Fig. 2, and the linewidth (*empty squares*) of the *three outermost lines* on the *right-hand side* of the spectra at the irradiating frequencies of 190 GHz for mTEMPO in $PDMS_q$. The *vertical dashed lines* mark the glass transition (148 K) and the cold crystallization (184 K) temperatures. The *superimposed dashed line* in the glassy region is the linear fit $\Delta B = a + bT$, with a = 311 ±1 G and $b = -0.091 \pm 0.002$ G/K

crystalline fraction. To understand the slowing down of the probe, we consider both the probe size and the interactions between the probe and the polymer. Let us first focus on the size. The estimates of mTEMPO and TEMPO volumes are 197 and 171 $Å^3$, respectively, i.e., mTEMPO is slightly larger than TEMPO [43]. In the spirit of the Stokes–Einstein law, the average reorientation scales with the volume of the spin probes [50]. Therefore, since the ratio between the reorientation times of mTEMPO and TEMPO is found to be about a factor of three, we conclude that the slightly larger mTEMPO volume alone is not enough to account for the slower mTEMPO reorientation. To proceed, a detailed analysis of the different kinds of interaction between distinct groups of the guest molecules and PDMS chain is summarized in Table 2. The spin probes interact with PDMS through van der Waals forces, i.e., (1) dipole–dipole interactions, (2) dispersion forces, involving non polar groups, and (3) induction forces, arising from a permanent dipole inducing a temporary dipole in a second group [51]. The interaction of N–O dipole with PDMS is neglected, because the nitroxide dipole is buried by the four methyl groups in positions 2 and 6. Table 2 suggests that mTEMPO is better coupled to PDMS than TEMPO due to the methoxy group where one additional methyl group and one permanent dipole are located. One also notices that the dipole–dipole force, differently from the dispersion and the induction forces, is very anisotropic. As a consequence, if the permanent dipoles are nearly free to rotate (Keesom interaction), a thermal averaging of the interaction takes place [51]. Close to the crystallite, both the spin probe and the PDMS segments are highly constrained and thermal averaging is anticipated to be less effective, thus resulting in stronger interaction, see Table 2. On this basis, one expects that, if mTEMPO and TEMPO are equally close to the crystallite, the former slows down the reorientation much more. The above analysis of the different mobility of the two spin probes is not conclusive and should be substantiated by, e.g., numerical simulations which are beyond our

Table 2 Van der Waals interactions between specific groups of mTEMPO and TEMPO and PDMS monomer or methyl groups

PDMS	Spin probe	Interaction	Energy (J/mol)	mTEMPO	TEMPO
Monomer	C-O-CH_3	D_p–D_p	870[a]	•	
Monomer	C-O-CH_3	D_p–D_p	69th	•	
CH_3	C-O-CH_3	D_i–D_p	13	•	
CH_3	C-O-CH_3	D_i–D_i	478	•	
Monomer	C-O-CH_3	D_p–D_i	10	•	
CH_3	CH_3	D_i–D_i	185		•
Monomer	CH_3	D_p–D_i	4		•

The table lists the kind of dipole (D_p and D_i denote permanent and induced dipole, respectively) and the energy at 5 Åspacing between the dipoles according to Ref. [51] with $\mu_{C-O-CH_3} = 1.29D$ and $\mu_{monomer} = 0.7D$ [52, 53]. Ionization energy (10 eV) and polarizability ($\alpha_{CH_3}/4\pi\epsilon_0 = 2 \times 10^{-30}$ m^3) of the methyl group from Ref. [54]. Polarizability ($\alpha_{C-O-CH_3}/4\pi\epsilon_0 = 5.16 \times 10^{-30}$ m^3) of the C-O-CH_3 group from Ref. [55]

[a] Aligned parallel monomer and C-O-CH_3 dipoles

[b] Thermally averaged dipole orientation (Keesom interaction, T = 220 K)

present purposes. Our tentative conclusion is that the slower rotational mobility of mTEMPO with respect to TEMPO follows from a combination of stronger interactions with PDMS and a slightly larger size.

3.3 Models of the Rotational Dynamics

Following the previous studies on the influence of the rotational dynamics on the EPR signal [56] in crystalline polymers [35] and viscous liquids [7, 57], a thorough numerical analysis of the HF-EPR lineshape has been performed. Below 200 K a simple model, referred to as single reorientation time (SRT) model, adopting a single average reorientation time τ_{SRT} satisfactorily predicts the lineshape, see Fig. 4. Differently, above 200 K, the SRT model becomes inadequate (not shown). We ascribe the failure of the SRT model to two different reasons: (1) the larger sensitivity of HF-EPR to the rotational dynamics when the temperature increases; (2) the presence of a distribution of environments where the spin probes are located leading to a distribution of the rotational mobility. With the purpose of improving the SRT model, above 200 K, we consider the lineshape $L(B)$ as a weighted superposition of contributions:

$$L(B) = \int_0^\infty L(B,\tau) \cdot \rho(\tau)\, \mathrm{d}\tau, \tag{1}$$

where $L(B,\tau)$ is the EPR lineshape corresponding to reorientation time τ and $\rho(\tau)$ is a suitable distribution of reorientation times.

As a first step, we considered the power-law distribution (PD):

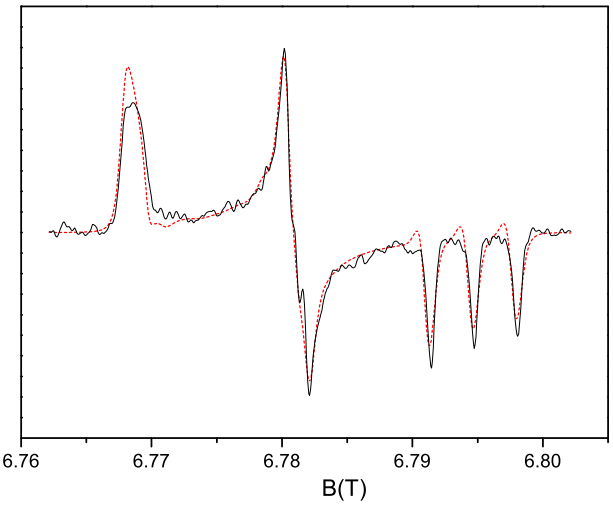

Fig. 4 Experimental (*black line*) and simulated (*red short dot line*) HF-EPR spectra of paramagnetic probe in $PDMS_q$ at 164 K and an irradiating frequency of 190 GHz. The simulation was performed using a single reorientation time, with τ_{SRT} = 123 ns. The small discrepancy between the simulation and the peak at low magnetic field was already noted [13] (color figure online)

$$\rho_{PD}(\tau) = \begin{cases} 0 & \text{if } \tau < \tau_{PD} \\ x \cdot \tau_{PD}^{x} \cdot \tau^{-(x+1)} & \text{if } \tau \geq \tau_{PD}, \end{cases} \tag{2}$$

where τ_{PD} is the shortest reorientation time and x is related to the distribution width. Even if successful for TEMPO in $PDMS_{sc}$, [13] the application of the PD model to mTEMPO in $PDMS_q$ leads to disappointing results. In fact, the x parameter was found to be as low as 0.1, which would imply that reorientation times longer than 100 ns have a significant weight in the distribution ρ_{PD}. Since HF-EPR is not sensitive to such slow reorientation, any model of the distribution $\rho(\tau)$ in the region $\tau \gtrsim$ 100 ns is flawed. Then, the identification $\rho \simeq \rho_{PD}$ was deemed as not consistent and the PD model was rejected.

To improve the PD model, we compared the HF-EPR spectra of mTEMPO in $PDMS_q$ with those of TEMPO in $PDMS_{sc}$ at both 190 and 285 GHz in Fig. 2 (lower traces). The observed mismatch suggests the presence of a trapped fraction of mTEMPO in $PDMS_q$, which we call δ, undergoing quite slow reorientation. We characterize the reorientation of the δ fraction by a single, relatively long reorientation time, $\tau_{trapped}$, and model the overall distribution of the reorientation times of both the trapped and the untrapped fractions, ρ_{PDT}, as a weighted sum of the δ component and a PD component:

$$\rho_{PDT}(\tau) = w_{PD} \cdot \rho_{PD}(\tau) + (1 - w_{PD}) \cdot \delta(\tau - \tau_{trapped}), \tag{3}$$

where $\delta(x)$ is the Dirac delta and w_{PD} is a weighting factor. Figure 5 shows an illustrative example of the best-fit provided by the PDT model. It must be noted that using the PDT model for mTEMPO in $PDMS_q$ yields values of the x parameter comparable to the ones found for TEMPO in $PDMS_{sc}$. As an example, at 203 K, one

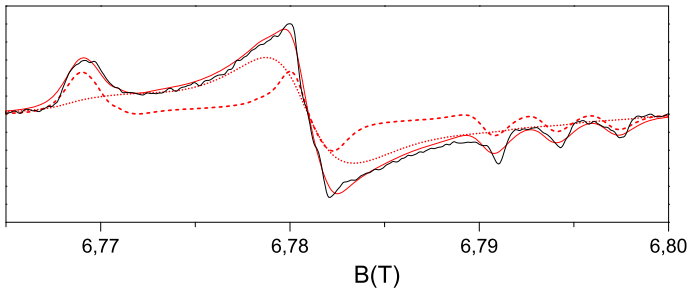

Fig. 5 Experimental HF-EPR spectra at 190 GHz of the spin probe in $PDMS_q$ at 222 K (*continuous black line*) compared to the best fit according to the PDT model, Eq. 3 (*continuous red line*). The contributions due to the PD and δ components of $\rho_P DT$ are superimposed as *short-dotted* and *short-dashed lines*, respectively. The best-fit parameters are $\tau_{PD} = 0.33$ ns, $x = 0.9$, $\tau_{trapped} = 21$ ns, and $w_{PD} = 0.62$ (color figure online)

finds $x = 0.67$ and $x = 0.68$ for mTEMPO and TEMPO, respectively. This consistency reassured us about the reliability of the PDT model.

Figure 6 (top) shows representative plots of the $\rho_{PDT}(\tau)$ distribution of mTEMPO. One sees that the broad component is well separated by the trapped one. Figure 6 (bottom) shows the same distribution for TEMPO [13]. It is seen that no trapped fraction is apparent and the distribution is shifted at shorter reorientation times than mTEMPO confirming that the latter has lower rotation mobility.

The agreement of the PDT model with the experiment covered the range between 200 K and T_m.

3.4 Evidence of RAF

We are now in a position to characterize the rotational dynamics of the trapped fraction of mTEMPO in $PDMS_q$. The results are summarized in Fig. 7.

From the lowest temperatures below T_g, passing through T_{cc}, up to about 200 K, the probe exhibits homogeneous dynamics well accounted by the SRT model. It has to be noted that the absence of any discontinuity of τ_{SRT} at $T_{cc} \sim 184$ K indicates that the probe does not sense the formation of the crystallites occurring on heating during data collection. The reorientation time τ_{SRT} slowly decreases on increasing the temperature. An Arrhenius fit provides an activation energy of 6.2 ± 0.3 kJ/mol in agreement with a value of 6.4 kJ/mol found for methyl jumps in PDMS [58]. This suggests coupling between mTEMPO and local modes. As pointed out in Sect. 3.3, on approaching the onset of PDMS melting (≃209 K), the heterogeneity of the reorientation of mTEMPO becomes apparent. The complete analysis will presented elsewhere. Here, we concentrate on the trapped fraction of mTEMPO, being characterized by a single reorientation time $\tau_{trapped}$. Figure 7 shows that the reorientation time $\tau_{trapped}$ joins smoothly with the single reorientation time τ_{SRT} characteristic of the spin probe reorientation below $\sim T_g$ and exhibits, up to T_m, the *same* temperature dependence. These findings suggest that, on increasing the temperature above 200 K, a part of the guest molecules persists in the glassy dynamics up to T_m. The presence of a glassy fraction of mTEMPO between T_{cc} and

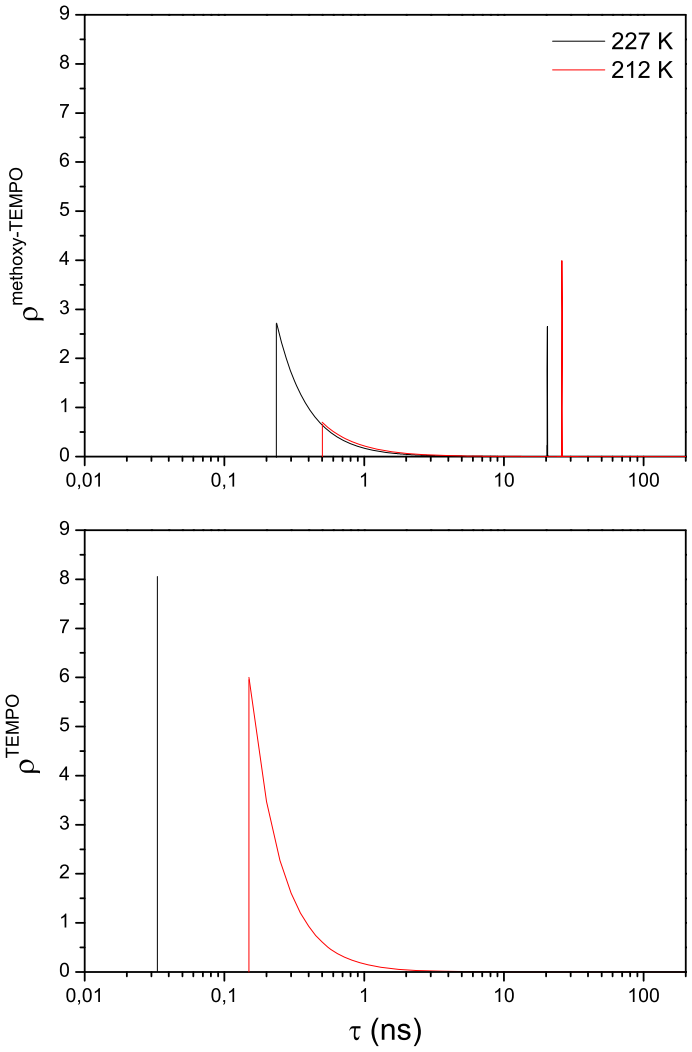

Fig. 6 Distributions of the reorientation times of mTEMPO (*top*) and TEMPO (*bottom*) [13] in the PDMS melting region according to the reorientation models. The best-fit parameters for mTEMPO are at $T = 212$ K, $x = 0.70$, $\tau_{PD} = 0.50$ ns, $\tau_{trapped} = 26$ ns, $w_{PD} = 0.51$, $T = 227$ K, $x = 0.92$, $\tau_{PD} = 0.23$ ns, $\tau_{trapped} = 20$ ns, and $w_{PD} = 0.70$. For TEMPO at $T = 212$ K, $x = 0.9$, $\tau_{PD} = 0.15$ ns, $w_{PD} = 1$ and at $T = 227$ K, and $\tau_{SRT} = 0.033$ ns. The peaks located on the *left* and the *right sides* of the power-law component mark the single reorientation time in the homogeneous reorientation regime of TEMPO in $PDMS_{sc}$ and the trapped δ component of mTEMPO in $PDMS_q$, respectively

T_m is striking evidence that the spin probe is located in RAF [3]. The untrapped, faster fraction is attributed to spin probes located in MAF and in a region with an intermediate mobility between that of the glassy fraction and of MAF.

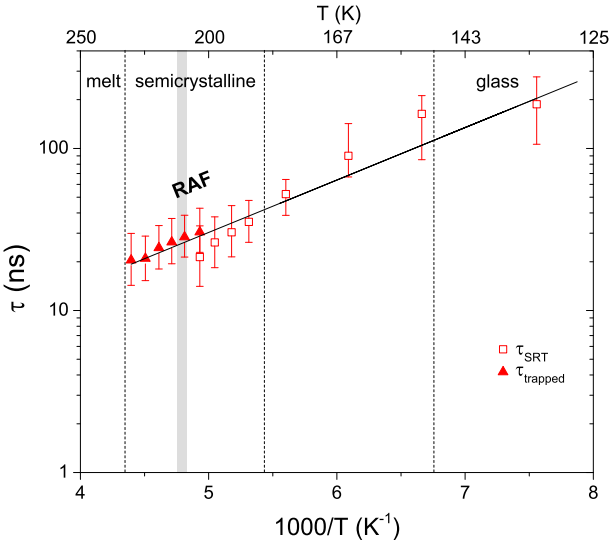

Fig. 7 Temperature dependence of the characteristic times τ_{SRT} and $\tau_{trapped}$ of mTEMPO in $PDMS_q$. The *dashed vertical lines* mark the glass transition at T_g, the cold crystallization at T_{cc}, and the melting transition at T_m, whereas the *gray region* highlights the range of the onset of PDMS melting ($\simeq$209 K). The *straight line* is an Arrhenius fit with an activation energy 6.2 $\pm$ 0.3 kJ/mol

All in all, the present results support the conclusion that mTEMPO in $PDMS_q$ provides more insight about RAF than TEMPO in $PDMS_{sc}$ thanks to both the better coupling of the spin probe and the thermal protocol enhancing the amount of RAF.

4 Conclusions

The reorientation of mTEMPO spin probe in semicrystalline quench cooled PDMS has been investigated by means of HF-EPR spectroscopy at two different Larmor frequencies (190 and 285 GHz). The guest molecule is confined outside the crystallites. Numerical simulation of the lineshape evidences that the rotational dynamics is well accounted for by a single effective reorientation time τ_{SRT} in the glassy region and up to about 200 K. The related activation energy suggests that the spin probe is coupled to local motions. Above 200 K, the spin probe exhibits a distribution of reorientation times $\rho(\tau)$ with bimodal structure characterized by (1) a broad component corresponding to states with fast and intermediate rotational mobility and (2) a narrow component corresponding to a fraction of guest molecules with extremely low rotational mobility. The finding that the reorientation time of the spin probes with low mobility and in glassy PDMS exhibits the same temperature dependence suggests that the low-mobility fraction is localized in the so-called rigid amorphous fraction.

Acknowledgements Helpful discussions with Monica Bertoldo, Giacomo Prampolini, and Maria Cristina Righetti are gratefully acknowledged.

References

1. G.R. Strobl, *The Physics of Polymers*, III edn. (Springer, Berlin, 2007)
2. U.W. Gedde, *Polymer Physics* (Chapman and Hall, London, 1995)
3. B. Wunderlich, Prog. Polym. Sci. **28**, 383 (2003)
4. G. Strobl, Prog. Polym. Sci. **31**, 398 (2006)
5. C. Schick, Anal. Bioanal. Chem. **395**, 1589 (2009)
6. H. Adachi, K. Adachi, Y. Ishida, T. Kotaka, J. Polym. Sci. Pt. B-Polym. Phys. **17**, 851 (1979)
7. A. Barbieri, G. Gorini, D. Leporini, Phys. Rev. E **69**, 061509 (2004)
8. M. Roos, K. Schäler, A. Seidlitz, T. Thurn-Albrecht, K. Saalwächter, Colloid Polym. Sci. **292**, 1825 (2014)
9. K. Schmidt-Rohr, H.W. Spiess, *Multidimensional Solid-State NMR and Polymers* (Academic Press, London, 1994)
10. A. Alegria, J. Colmenero, Soft Matter **12**, 7709 (2016)
11. M.M. Dorio, J.C.W. Chien, Macromolecules **8**, 734 (1975)
12. S. Kutsumizu, M. Goto, S. Yano, Macromolecules **37**, 4821 (2004)
13. C.A. Massa, S. Pizzanelli, V. Bercu, L. Pardi, D. Leporini, Macromolecules **47**(19), 6748 (2014)
14. C.A. Massa, S. Pizzanelli, V. Bercu, L. Pardi, M. Bertoldo, D. Leporini, Appl. Magn. Reson. **45**, 693 (2014)
15. L.J. Berliner, J. Reuben (eds.), *Biological Magnetic Resonance* (Plenum, New York, 1989)
16. R. Ross, J. Chem. Phys **42**, 3919 (1965)
17. J.S. Leigh Jr., G.H. Reed, J. Phys. Chem. **75**, 1202 (1971)
18. M.K. Ahn, J. Chem. Phys. **64**, 134 (1976)
19. D. Banerjee, S.N. Bhat, S.V. Bhat, D. Leporini, Proc. Natl. Acad. Sci. USA **106**, 11448 (2009)
20. D. Banerjee, S.N. Bhat, S.V. Bhat, D. Leporini, PLoS One **7**, e44382 (2012)
21. D. Banerjee, S.V. Bhat, D. Leporini, Adv. Chem. Phys. **152**, 1 (2013)
22. R.F. Boyer, Polymer **17**, 996 (1976)
23. P. Törmälä, J. Macromol. Sci. Part C **17**, 297 (1979)
24. G.G. Cameron, in *Comprehensive Polymer Science*, ed. by C. Booth, C. Price (Pergamon Press, Oxford, 1989), pp. 517–542
25. B. Rånby, J. Rabek, *ESR Spettroscopy in Polymer Research* (Springer, Berlin, 1977)
26. M. Faetti, M. Giordano, D. Leporini, L. Pardi, Macromolecules **32**, 1876 (1999)
27. D. Leporini, V. Schädler, U. Wiesner, H.W. Spiess, G. Jeschke, J. Chem. Phys. **119**(22), 11829 (2003)
28. V. Bercu, M. Martinelli, C.A. Massa, L.A. Pardi, D. Leporini, J. Phys.: Condens. Matter **16**, L479 (2004)
29. V. Bercu, M. Martinelli, L. Pardi, C.A. Massa, D. Leporini, Z. Phys. Chem. **226**, 1379 (2012)
30. V. Bercu, M. Martinelli, C.A. Massa, L.A. Pardi, D. Leporini, J. Chem. Phys. **123**, 174906 (2005)
31. N.G. McCrum, B.E. Read, G. Williams, *Anelastic and Dielectric Effects in Polymeric Solids* (Dover Publications, New York, 1991)
32. K.U. Kirst, F. Kremer, V.M. Litvinov, Macromolecules **26**, 975 (1993)
33. K.L. Ngai, *Relaxation and Diffusion in Complex Systems* (Springer, Berlin, 2011)
34. K.L. Ngai, C.M. Roland, Macromolecules **26**, 2688 (1993)
35. L. Larini, A. Barbieri, D. Prevosto, P.A. Rolla, D. Leporini, J. Phys.: Condens. Matter **17**, L199 (2005)
36. M. Cocca, M.L.D. Lorenzo, M. Malinconico, V. Frezza, Eur. Pol. J. **47**, 1073 (2011)
37. M. Drieskens, R. Peeters, J. Mullens, D. Franco, P.J. Lemstra, D.G. Hristova-Bogaerds, J. Polym. Sci Part B: Polym. Phys. **47**, 2247 (2009)
38. S.C. George, S. Thomas, Prog. Polym. Sci. **26**, 985 (2001)
39. M. Klopffer, B. Flaconnèche, Oil Gas Sci. Technol. **56**, 223 (2001)
40. J.H. Freed, Annu. Rev. Phys. Chem. **51**, 655 (2000)
41. K.A. Earle, D.E. Budil, J.H. Freed, J. Phys. Chem. **97**, 13289 (1993)
42. J.W. Saalmueller, H.W. Long, T. Volkmer, U. Wiesner, G.G. Maresch, H.W. Spiess, J. Polym. Sci. Pt. B-Polym. Phys. **34**(6), 1093 (1996)
43. A.C. Soegiarto, W. Yan, A.D. Kentab, M.D. Ward, J. Mater. Chem. **21**, 2204 (2011)
44. H.B. Eitouni, N.P. Balsara, in *Physical Properties of Polymers Handbook*, II edn., ed. by J.E. Mark (Springer, Berlin, 2007), pp. 339–356

45. X. Wang, J. Ouyang, Int. J. Chem. Eng. Appl. **6**, 28 (2015)
46. H. St-Onge, I.E.E.E. Trans, Electr. Insul. **EI–15**, 359 (1980)
47. L.C. Brunel, A. Caneschi, A. Dei, D. Friselli, D. Gatteschi, A.K. Hassan, L. Lenci, M. Martinelli, C.A. Massa, L.A. Pardi, F. Popescu, I. Ricci, L. Sorace, Res. Chem. Intermed. **28**(2–3), 215 (2002)
48. M. Giordano, P. Grigolini, D. Leporini, P. Marin, in *Memory Function Approaches to Stochastic Problems in Condensed Matter*, ed. by M.W. Evans, P. Grigolini, G.P. Parravicini (Wiley, New York, 1985), pp. 321–388
49. L. Alessi, L. Andreozzi, M. Faetti, D. Leporini, J. Chem. Phys. **114**, 3631 (2001)
50. L. Andreozzi, A.Di Schino, M. Giordano, D. Leporini, Europhys. Lett. **38**, 669 (1997)
51. P. Atkins, J. de Paula, *Atkins' Physical Chemistry* (Oxford University Press, Oxford, 2010)
52. K. Matsumura, Bull. Chem. Soc. Jpn. **35**, 801 (1962)
53. A.C.M. Kuo, in *Polymer Data Handbook*, ed. by J.E. Mark (Oxford University Press, Oxford, 1999), pp. 411–435
54. Y.K. Kang, M.S. Jhon, Theor. Chim. Acta **61**, 41 (1982)
55. C.G. Gray, K.E. Gubbins, *Theory of Molecular Fluids*, vol. 1 (Clarendon Press, Oxford, 1984)
56. D. Leporini, Phys. Rev. A **49**, 992 (1994)
57. L. Andreozzi, M. Faetti, M. Giordano, D. Leporini, J. Phys. Chem. B **103**, 4097 (1999)
58. H.H. Grapengeter, B. Alefeld, R. Kosfeld, Colloid Polym. Sci. **265**(3), 226 (1987)